Analysis of Myosin XI and RabA Relationships during Polarized Tip Growth in *Physcomitrella patens*

A Major Qualifying Project
Submitted to the Faculty of
WORCESTER POLYTECHNIC INSTITUTE
In Partial Fulfillment of the Requirements for the
Degree of Bachelor of Science
By:

Kelsi Callahan

Date:

May 1, 2014

Approved:

Professor Luis Vidali

Worcester Polytechnic Institute

Abstract

In plants, polarized tip growth is a fundamental process that occurs by the myosin-dependent transport of secretory vesicles to the growing tip. It is believed that Rab proteins play a role as myosin receptors on secretory vesicles. To evaluate this hypothesis, I performed fluctuation cross-correlation analysis to characterize the spatiotemporal relationship between myosin and RabA proteins in *Physcomitrella patens*. Supporting the hypothesis, I found a strong correlation of the fluctuations levels between both proteins at the tip of growing cells.

Acknowledgements

This project was accomplished with the assistance of a number of individuals. I would like to thank Dr. Fabienne Furt for her constant guidance in the lab as well as for providing feedback on the report draft. In addition, I would like to thank my advisor Dr. Luis Vidali for his advice and feedback throughout the project. I would also like to thank Jeff Bibeau for his MatLab programs which allowed for the statistical analysis of the data. Also thank you to all of the members of the Vidali lab, including Scott Doherty, Hao Sun, Xinxin Ding, Divya Panickar, Benjamin Pulver, and Maria Luckette, for their feedback and various help around the lab. I would also like to acknowledge and thank everyone at Gateway who allowed me to use the lab, its resources, and its equipment.

Table of Contents

1. Introduction

1.1 Background on Polarized Growth

Cell growth is a process during which a cell develops and expands before replication. In studying the variety of mechanisms behind cell growth, we can potentially use this knowledge for beneficial purposes. For example, learning how a tumor cell grows and functions can lead to finding a method to halting this growth in a patient where these cells are harmful. Studying cell growth also has its benefits in agriculture. Water and nutrient uptake, for example, are fundamental process for plants that relies on a process known a tip growth. By learning more about this growth process we could potentially increase the growth and size of these agricultural plants.

When conceptualizing the growth of an average cell, one may imagine a cell expanding by diffuse growth in which growth material is deposited uniformly and the cell expands in all directions. However in certain cell types, growth material may only be deposited at one side of the cell causing non-uniform expansion which is known as polarized growth. For example, epithelial cells in animals grow in only two directions towards either the apical side (facing the outer body surface) or the basal side (facing the inner tissue) of the cell. When polarized growth occurs in a single direction of a cell, rapidly elongating the cell cylindrically it is known as tip growth. Polarized tip growth can be observed in a variety of both animal and plant cell types such as neuron and root hair cells respectively. In studying the molecular mechanisms behind polarized tip growth, this process of cellular expansion can be better understood.

There are various cellular processes that contribute to polarized tip growth including the cytoskeleton and the endomembrane system. The cytoskeleton is generally referred to as the scaffolding of the cell and assists in the transport of organelles and materials within the cell. The endomembrane system consists of various internal membranes contained within the cytoplasm of an eukaryotic cell, which include organelles such as Golgi bodies, vacuoles, and the plasma membrane. This system is often connected by the exchanging of material through the transport of vesicles. The movement of vesicles from the endoplasmic reticulum, to the Golgi and then to the plasma of the cell is known as the exocytic pathway. This trafficking of vesicles through the cell provides material for expansion and elongation of the plasma membrane and has been found to be a critical process in cellular growth, including polarized pollen tube growth (Zang and McCormick, 2010). Therefore during polarized growth, secretory vesicles containing cell wall material from the Golgi are transported via the cytoskeleton and are deposited into the plasma membrane via exocytosis at the area of expansion.

Although this basic mechanism is understood, the specifics on how this system is regulated are still not clearly known. Previous research has established that the actin cytoskeleton plays a necessary role in plant polarization and growth and that the motor protein myosin assists in the transport of vesicles along F-actin (Furt et al., 2013). Myosin is a protein that moves along the actin cytoskeleton and contains a cargo binding domain in order to bind to and help transport various organelles and vesicles within the cell. There are different types of myosins present in the cell depending on the organism. Recent research has found that the class XI myosin found in plants may play a predominant role in polarized growth (Vidali et al., 2010; Peremyslov et al., 2010).

However if this is the case, it is still unclear how this myosin correctly binds to transport vesicles in order to carry them to the site of cell expansion and growth. In order to further investigate the role of these myosin XIs, a plant-based model organism is needed for further study.

1.2 *Physcomitrella patens* as a Model Organism

In order to further study the process and mechanisms behind polarized growth, a simple plant model organism known as *Physcomitrella patens (P. patens)* can be used. *P. patens* is a particular species of moss (or bryophyte) and is a useful model to study plant development and evolution. Although sometimes overlooked, mosses are an important group of plants and represent one of the earliest plants that began colonizing on land and helped make way for the more complex, flowering plants of today.

Among the variety of mosses, *P. patens* is studied predominantly for its suitable role in genetic analysis (Goffinet and Shaw, 2009). This is due to the fact that moss undergoes efficient non-meiotic homologous recombination; a process in which DNA that contains sequences similar or identical to sequences found in the organism's genome will preferentially recombine at that genomic site. Genetic recombination of *P. patens* was found to be possible with significantly high success rate (Schaefer and Zryd, 1997) making it a desirable model for targeting specific genes and then using reverse genetics to determine the function of that gene by observing a mutant phenotype. In addition, the complete genome of *P. patens* has recently been sequenced allowing for the comparison of genomic features across various plant species (Rensing et al., 2008; Beike and Rensing, 2010). For these reasons, *P. patens* has become widely adopted as

a model organism for genetic based studies of plant processes and evolutionary development.

Like all mosses, the dominant phase of this organism's life cycle is its leafy, haploid gametophyte stage. Nevertheless, the first type of tissue to begin growth from the spore is protonemata. After spore germination, protonemal filaments begin to burst and branch out from the plant, exclusively growing in a polarized tip growth fashion (Vidali and Bezanilla, 2012). Hence in its beginning protonemal phase of growth, *P. patens* cells grow exclusively by tip growth. The initial cell types to from after spore germination are chloronema. Chloronemal cells contain a relatively large number of chloroplasts, have a rounded apical tip, are relatively slow growing, and can be distinguished by perpendicular cell walls. Differentiating off from these is a second type of protonemal filament known as caulonema. Caulonemal cells contain relatively fewer chloroplasts, have a more pointed apical tip, are relatively fast growing, and can be distinguished by oblique cell walls. Because the caulonemal filaments are faster growing, these were the cell types used for most cell biological studies.

In studying polarized growth in *P patens,* the accepted hypothesis was that the motor protein myosin transported secretory vesicles to the areas of growth along the actin cytoskeleton. This was due to the observation that when myosin was silenced, *P. patens* plants would exhibit small, round cells not capable of polarized growth (Vidali et al., 2010). This actin cytoskeleton was also assumed to be established and organized prior to myosin transportation. However in recent studies, it was found that the accumulation of myosin at tip of the cell leads the accumulation of F-actin at the site of tip growth, suggesting that myosin may help to organize actin polymerization at the tip

(Furt et al. 2013). Figure 1 shows a hypothetical model that explains the mechanism behind tip growth based on these recent observations. Interestingly, this suggests that endomembrane vesicles may not only act as cargo, but may also help to organize myosin and actin at the tip of the moss cells.

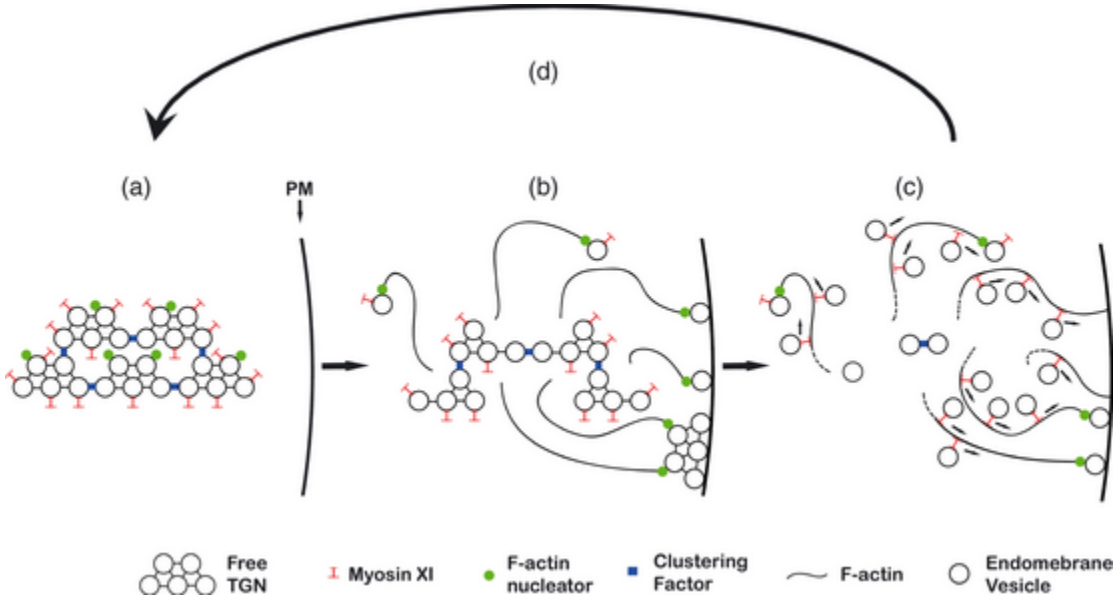

Figure 1: Hypothetical model explaining myosin, actin, and vesicle behavior at the site of polarized tip growth (Furt et al. 2013)

1.3 Background on Cytoskeleton and Myosin

It was originally believed that the long range transport of vesicles within animal cells occurred via the microtubules; however evidence has suggested that this process may be more dependent on the presence of actin within the cell (Schuh, 2011). In plant

cells, the actin cytoskeleton also holds an important role in intracellular transport, and plays a critical role in polarized growth (Furt et al., 2013). There are two main types of cytoskeletal filaments in plants: the microtubules and the microfilaments (also known as actin filaments).

Microtubules are long, hollow cytoskeleton tubes that are made up of α and β tubulin dimers. These dimers then polymerize at their ends to form protofilaments. A microtubule consists of thirteen protofilaments that are wrapped around in a polar, helical structure. Microtubules are typically associated with processes involving intracellular transport, mitosis, and organelle positioning (Huber et al., 2013).

Actin consists of individual monomers which are small, globular proteins (G-actin), and these monomers can then bind and form linear polymers (called F-actin or microfilaments). These microfilaments both actively polymerize and depolymerize within the cell depending on a variety of intracellular processes regulated by actin binding proteins, and this is referred as the actin dynamics. Due its dynamic nature, actin filaments are typically associated with determining the shape of the cell and polarized growth (Huber et al., 2013).

Also associated with actin filaments is the motor protein myosin. This protein typically functions as a dimer consisting of two motor, or head, domains. These head domains allow the protein to move through the cell by associating with actin filaments via ATP hydrolysis. In addition to this head, in myosin XI there is also a neck region, a coil-coil tail region thought to be needed for the dimerization of the protein, and a cargo binding tail region (Figure 2). Based on phylogenic analysis across different organisms, 35 different classes of myosin have been identified based on their functions (Maravillas-

Monero and Santos-Argumedom, 2012). Land plants contain only two classes of myosin, myosin VIII and myosin XI. Interestingly, the myosin XI found in plants is a homolog of myosin V found in animals and fungi. One of the benefits of studying myosin XI in *P patens* is that there are only two types of myosin XI (myosin XIa and myosin XIb) (Vidali et al., 2010). Arabidopsis plants on the other hand contain thirteen different types of myosin XIs (Hashimoto et al., 2005). Thus using *P patens* as a model organism is advantageous and simplifies the study of myosin XI.

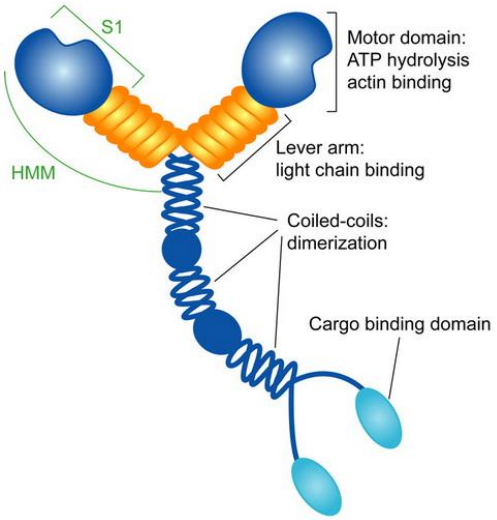

Figure 2: Basic structure of myosin V, a homolog to plant myosin XI (Tóth et al., 2005)

Along with long range transport of vesicles, actin and myosin play a necessary role in plant polarization and growth. In *P. patens*, studies have shown that fluorescent intensities of myosin XI fluctuate in phase with fluorescent intensities of v-SNARE proteins found in transport vesicle membranes (Furt et. al, 2013). These in phase fluctuations suggested a paired correlation, and this provides evidence that myosin XI associates with vesicles during transport. *P patens* that had myosin XI silenced, along

improper growth, also lacked proper F-actin organization providing evidence for myosin's importance polarized tip growth and F actin organization (Furt et al., 2013).

Similar results have been found in other plant types as well, including diminished root hair growth in *Arabidopsis* plants which also grows in a polarized, tip growth fashion (Park et. al, 2013). More specifically, it has been shown that by knocking out a number of different class XI myosins, *Arabidopsis* exhibited stunted growth along with abnormal root hair development (Peremyslov et al,. 2010). Another interesting result of this study was that the trafficking of Golgi and the organization of actin were also myosin dependent.

1.4 Rab Proteins

Rabs are a family of GTPase proteins, which are in their active state when bound to GTP and in their inactive when bound to GDP. Rab proteins are important for membrane targeting and contain interaction surfaces that help regulate the movement of the vesicles or organelles (Zerial and McBride, 2001). Because both Rab and Myosin are involved in organelle transport, it would be logical to conclude that Rab may also be involved in polarized growth processes along with myosin. This has been found to be true in both animal and budding yeast cells (Itoh et al., 2002; Wu et al., 2002) but has yet to be shown in plants.

Although various classes of Rab proteins have been found to be conserved across species, their nomenclature often depends on the organism they are found in. For example, the Rab proteins that are located in post-Golgi compartments/vesicles

may be classified as the Rab11 in animals, Ypt32 in yeast, and RabA in plants. These specific Rab GTPases play an important role in membrane identification and targeting which is needed for proper trafficking of plant organelles and vacuoles (Woollard and Moore, 2008). In yeast, there is evidence that Rab proteins such as Sec4 and Ypt31/31 interact with myosin V in order to regulate organelle transport within the cell (Seabra and Coudrier, 2004; Lipatova et al., 2008). In Arabidopsis pollen tubes, RabA4d is found to be localized at the tip and when this specific Rab was deleted, the pollen tubes appeared shorter and grew at a slower rate (Feraru et al., 2012). These studies show that, like myosin, Rabs are important for organelle transport along with tip growth.

The interactions between Myosin and Rab have been studied in both animal and yeast cells. In animal cells, organelles known as melanosomes are responsible for the transport and storage of melanin and are bound by a bi-lipid membrane. In order for this organelle to be transported, Rab27a is recruited to the melanosome membrane before binding to myosin-Va with the help of a carrier protein known as melanophilin (Wu et al., 2002). In the yeast *Saccharomyces cerevisiae*, a Rab protein known as Ypt31/32, located in post-Golgi vesicles, interacts with a class V myosin known as Myo2 in order to transport vesicles for polarized secretion (Lipatova et al., 2008). In addition, myosin Vb has also been found to associate with Rab11s to help regulate recycling of the plasma membrane (Hales et al., 2002). Myosin V is homologous in structure to plant myosin XI, therefore it seems likely that this interaction may also be conserved in plants, however this has yet to be fully demonstrated.

1.5 Purpose of this Study

The purpose of this study is to further attempt to identify the protein that plant myosin XI interacts with in order to tag and transport vesicles to the apex of polarized tip growing cells. Based off the knowledge and work of previous studies (Armstrong, 2012; Agar, 2013), the goal is to test the hypothesis that myosin XIa in *P. patens* interacts with at least one of the RabA family proteins. These Rabs have been narrowed down to RabA21, RabA4, and RabA53 which represent each of the RabA family subgroups that are present in *P. patens*. In addition, these observations aim to verify that the correlation between Rabs, myosin, and actin are similar to the correlation of v-SNARE proteins, myosin, and actin established in a previous study (Furt et al., 2012). Doing so will contribute to future work and help to further test the hypothesis that myosin XI interacts with one or multiple RabA proteins in order to facilitate polarized growth in *P. patens.*

2. Materials and Methods

2.1 Cell Lines

For the fluctuation cross correlation analysis, three different lines of moss containing two separate fluorescent fusion proteins were used. Two of these lines tagged myosin XI with 3mEGFP and RabA21 with 3mCherry. In the first line, labeled as **3mEGFP-Myosin+3mCherryRabA21**, the 3mEGFP was fused to the N terminus of the myosin XIa cDNA and this construct was overexpressed in moss cells. Consequently, these lines expressed both non-labeled endogenous myosin XIa and fluorescently labeled myosin XIa. In the second line, labeled as **Myosin-3mEGFPKI+3mCherry-RabA21**, the 3mEGFP was directly inserted at the endogenous locus after the C terminus of the myosin XIa gene. Therefore, these lines expressed only a fluorescently labeled myosin XIa at the endogenous level. The third line expressed Lifeact, N terminus-tagged, with 3mEFGP and RabA21 N terminus-tagged with 3mCherry. Lifeact is a small protein (17 amino acids) with a high affinity for binding to actin filaments. Therefore fluorescently marked Lifeact (LA2W) will indicate where F-actin filaments are being formed. This third line was labeled as **3mEGFP-LA2W+3mCherry-RabA21**. All three lines were generated prior to this MQPs start.

2.2 Sample Preparation

In order to perform live cell imaging under the confocal microscope for an extended period of time, these lines were cultured on “holey” slides. A diagram of a holey slide is shown in Figure 3. These slides were prepared by pouring 5mL of $PpNO_3$

agar media into a small dish containing a hole with a coverslip adhered to the outside bottom of the dish (MatTek). A small area void of media was also created at the center of the dish by placing down an inverted pipet tip before adding the media. After the solidification of the media, approximately 80uL of media was placed inside this small area in order to make a very thin, even layer of solid media. The components of the $PpNO_3$ agar media are shown in Table 1. A small sample of moss was then sterilely placed in the center on the thin layer and grown for approximately a week in a 25°C growth chamber.

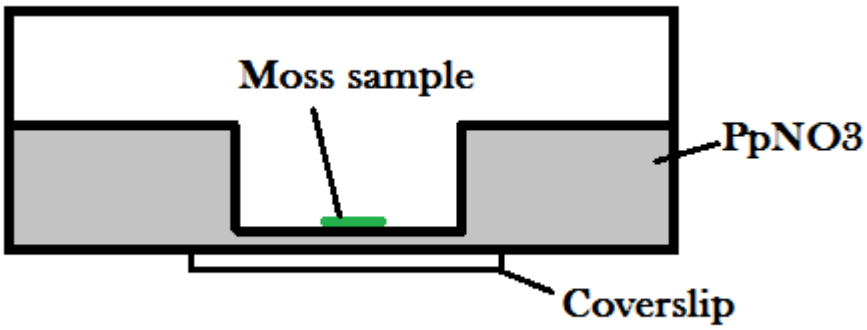

Figure 3: Diagram of holey slide

Table 1: Composition of Growth Media

Medium	**Composition**
Plating medium – $PpNO_3$	1.03mM $MgSO_4$ 1.86mM KH_2PO_4 3.3mM $Ca(NO_3)_2$ 45mM $FeSO_4$ 9.93mM H_3BO_3 220nM $CuSO_4$ 1.966mM $MnCl_2$ 231nM $CoCl_2$ 191nM $ZnSO_4$ 169nM KI 103nM Na_2MoO_4

2.3 Confocal Imaging

Once the moss cells were adequately grown, they were imaged under a SP5 confocal microscope (Leica), using a HCX-PL-Apo, 63x, NA 1.4 lens at 700 Hz. In order to examine both fluorescent proteins, two separate laser lines were used, one at 488nm to excite the 3mEGFP protein and the other at 561nm to excite the 3mCherry protein. To capture the emitted light, emission filters were tuned from 499-547nm for 3mEGFP and 547nm-652nm for 3mCherry. To reduce fluorophore photobleaching, the total laser power was kept at 6% for the 488nm laser and 4% for the 561nm laser. Straight, rapidly growing caulonemal cells were then identified visually; they must have an oblique cell wall and a clear zone at the tip. Their growth was recorded in a one hour-long movie, taking Z stack images (9 optical slices 1um apart) every five seconds. These Z stacks were compiled using average projections and then processed in ImageJ in order to create two separate time projection kymographs, one for each channel (Figure 4).

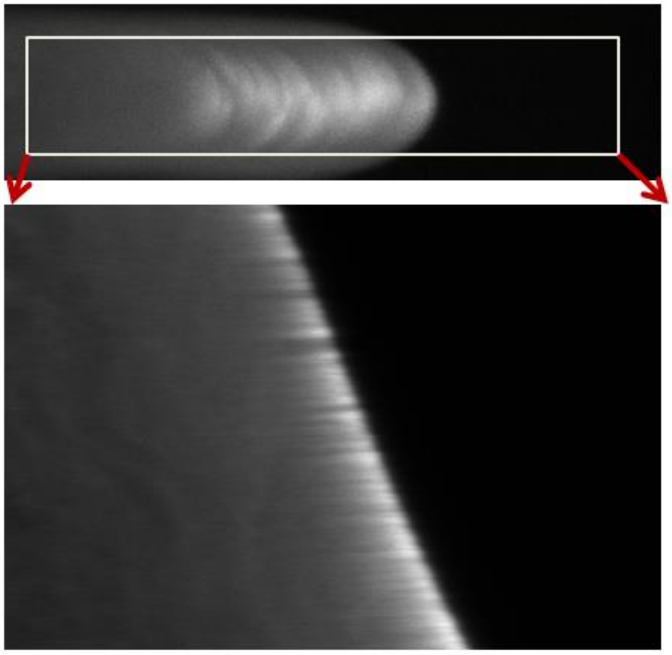

Figure 4: Kymograph of a fluorescently marked caulonemal cell over time. A time lapse (pictures top) was used to determine the region at which cell images were to be taken at each time interval (5 seconds). Time moves downward along the Y axis and the kymograph shows the shank, tip, and background region along the X axis.

2.4 Fluctuation Cross Correlation Analysis

These kymographs were then analyzed in MatLab to determine both the growth velocity and phase relation of the two channels. The growth rate was determined by measuring the slope of the fluorescent tip. In order to calculate the phase relation, the background intensity of the shank region of the cell and the region outside the cell were subtracted out and the intensity at the tip was then normalized at zero. The resulting intensity measurements were then de-trended using a Fourier series de-trending algorithm. The de-trended fluctuation signals were then compared in a cross correlation analysis at each time shift in order to determine the phase relation between the two signals. The equation for the cross-correlation analysis is shown below. S1 stands for signal 1, S2 stands for signal 2, t stands for time, and τ represents the time shift interval.

$$r(\tau) = \sum_{t=0}^{N-\tau} S_1(t)(S_2(t+\tau))$$

As a result, a correlation coefficient was produced at each time shift, and these measurements were then plotted over time. The program OriginPro was used to generate graphs and analyze standard error of this data.

2.5 Generation of RabA Constructs Fused to GST-tag

N-terminus GST-tagged Rab constructs were made in order to be expressed in bacteria to perform protein-protein interaction studies. A diagram outlining this process is shown in Figure 5. Total RNA was isolated from one week-old moss tissue using the "NucleoSpin RNA Plant" kit from Macherey-Nagel, following the manufacturer's protocol. A cDNA template for each corresponding Rab protein (RabA21, RabA4, and RabA53) was required for PCR however, as bacteria utilized in later cloning do not possess the enzymatic machinery necessary to splice and remove introns. Total cDNA was synthesized from total RNA using the SuperScript III reverse transcriptase (Life Technologies) and primed with an oligo(dT) primer, following the manufacturer's instruction. PCR was then used to amplify the cDNA corresponding to each Rab protein using the following primers shown in Table 2. These PCR products were then ran on a 0.8% agarose gel for 20 minutes at 220V. The expected size of RabA21, RabA4, and RabA53 cDNAs including the AttB1/B2 sites were 709, 727, and 710 bps respectively. The DNA was then extracted from the gel and purified using the Nucleospin Extract Kit from Macherey-Nagel. Entry clones were then generated via a BP Reaction using the

MultiSite Gateway System (Life Technologies). This was performed by mixing 7 ng of each PCR product, 75 ng of pDONR 221 vector and 1x TE buffer (pH8) to bring the mixture to 4uL (Table 3). 1ul of BP clonase enzyme was then added to start the reaction and this mixture was incubated at 25°C for 1 hour, after which 0.5 uL of Proteinase K solution was added to stop the reaction.

Table 2: List of Primers used to amplify Rab cDNAs

	Primer Sequences:
RabA21	AttB1:GGGGACAAGTTTGTACAAAAAAGCAGGCTTAATGGCGCACAAGGCCGACGACGAGT AttB2: GGGGACCACTTTGTACAAGAAAGCTGGGTACTAAGCTGAGCAACATCCCTT
RabA4	AttB1: GGGGACAAGTTTGTACAAAAAAGCAGGCTTAATGGCGAATGCGTACAATGAA AttB2: GGGGACCACTTTGTACAAGAAAGCTGGGTATTAACTTGAGCAACACCCTGC
RabA53	AttB1: GGGGACAAGTTTGTACAAAAAAGCAGGCTTAATGTCGTACCAGGATGAGCAG AttB2: GGGGACCACTTTGTACAAGAAAGCTGGGTACTAATACGAGCAGCACCCACC

Table 3: Composition of Buffer Media

Buffer:	**Composition**
TE Buffer (1x), pH 8.0	10mM Tris-HCl 1mM EDTA

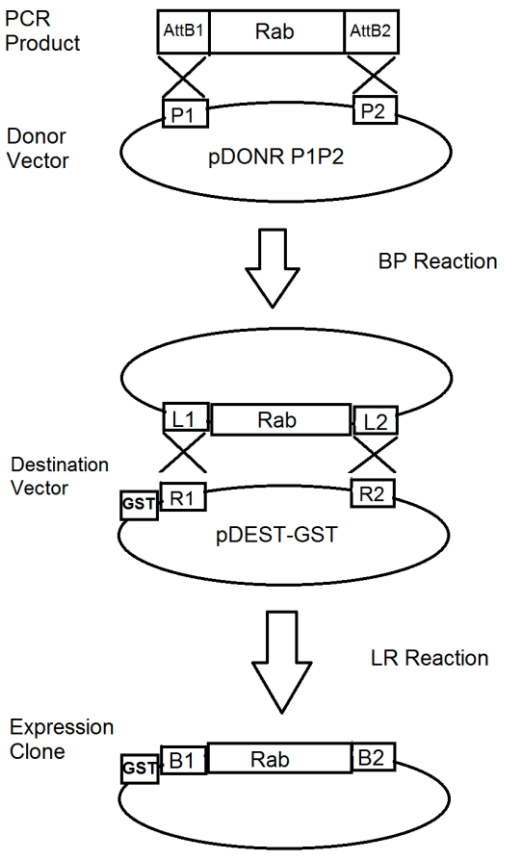

Figure 5: Diagram of Gateway system

Next, NEB 5-alpha chemically competent Escherichia coli (*E. coli*) cells (New England Biolabs) were transformed with this BP reaction mixture. 50uL of cells were first thawed on ice for 5 minutes before the entire BP reaction was added. These cells were then kept on ice for 30 minutes, heat shocked for 30 seconds at 42°C, and then placed back on ice for 5 minutes. Afterwards, 250ul of sterile LB medium was added and the cells were incubated in a rotating wheel for an hour at 37°C. After incubation, the cells were added to plates of solid LB and 50µg/ml of kanamycin and left at 37°C for approximately 12-14 hours. Growing colonies were then picked and incubated in 2mL of LB and kanamycin overnight at 37°C. The following day the plasmid DNA expressed by

the competent cells were isolated from the bacterial DNA and purified using a NucleoSpin Plasmid mini prep kit from Macherey-Nagel. The concentration of each plasmid was determined using a NanoDrop spectrometer from Thermo Scientific. Absorbance was measured at both 260 nm and 280nm to get an estimation of protein contamination. The concentration was calculated using the relation A_{260}=50ng/µl of DNA and corrected by the factor of dilution when necessary.

In order to verify that plasmids had the correct insert, they were digested with restriction enzymes for two hours at 37°C and were then ran through a 0.8% agarose electrophoresis gel (Results: Table 6). Clones correspond to the lanes showing the expected inserts were then sent in for sequencing using M13 forward and reverse primers. These primers are located just upstream of the Att sites framing the insert.

Once the sequences verified that the entry clones contained the proper inserts without mutations, they were then transferred into the pDEST-NTerm-GST vector using the MultiSite Gateway LR reaction. This was performed by mixing 70 ng of pDEST-NTerm-GST destination vector along with 65 ng of each entry clone plasmids in presence of 1x TE buffer to bring up to a final volume of 4ul. 1uL of LR Clonase was added to start the reaction and the mixture was left to incubate overnight at room temperature for approximately 16 hours. 0.5 uL of Proteinase K solution was then added to stop the reaction. Competent E. coli cells were then transformed with the entire LR reaction mixture, using a similar protocol to the BP reaction transformation, except that transformed cells were grown on plates containing LB and 100ug/ml of carbenicillin. Likewise, 2mL overnight cultures contained LB and carbenicillin. Mini preps were then made and the concentrations measured using the NanoDrop

spectrophotometer. Restriction digests were then performed and ran on a 0.8% agarose gel (Results: Table 7). Only one reaction was performed for cutting the ends of each insert, as there was no appropriate enzyme to cut inside the insert. Clones were then sequenced to confirm that the destination vectors contained the proper sequences.

2.6 *Physcomitrella patens* Transformation

Stable transformations were made using a 3mEGFPMyoKI#3 line in which the 3mEGFP was directly inserted at the endogenous locus after to the C terminus of the myosin gene (LV685). This line was transformed with a 3mCherryRabA53 DNA construct. In order to increase the efficiency of the transformation, this plasmid DNA was linearized by performing a SwaI restriction enzyme reaction. The SwaI reaction was performed by mixing 120ug of the DNA, 60ul of NEB Buffer 3, and 10ul of SwaI. This mixture was then incubated for 2-4 hours. Then 60uL of 3mNaAcetate was added along with 800ul of absolute ethanol. After being centrifuged, the DNA pellet was re-suspended in TE buffer. These transformations were performed by following the protocol summarized below (Luis and Vidali, 2011). The composition of the media used in the transformations is listed in Table 6 (Agar, 2013).

First, 9ml of 8% mannitol and 3ml of 2% driselase were added into a Petri dish. The moss to be transformed, grown for one week at 25°C, was then scrapped off the plate and incubated into the enzyme/mannitol mix in order to remove the plant's cell walls. After an hour, the obtained protoplasts were then filtered and transferred into a culture tube. The protoplasts were then pelleted by centrifuging in a swing-out rotor at 700rpm for 5 min. After pouring out the supernatant, 10ml of 8% mannitol was added to

the pellet and re-suspended by gentle inversion. This last step was repeated 2 more times to gently wash the cells. Then the number of protoplasts was determined using a hemocytometer. Cells were then centrifuged again, removing the supernatant and adding the appropriate volume of MMg medium (Transformation Media Table) to reach a final concentration of 1.6 x 10^6 protoplasts/ml of MMg. After re-suspension, protoplasts were left at room temperature for 20 minutes.

Solid PRMT medium containing 10mM of $CaCl_2$ was melted and kept in a water bath at 45°C. 600µl of protoplasts was then added to 120 µg of SwaI digested plasmid along with 700µl of PEG 4000/Ca. This protoplast and SwaI digested DNA mixture was left at room temperature for 30min. It was then diluted with 3ml of W5 medium (Transformation Media Table) and centrifuged for 5 min to remove PEG. Protoplasts were then re-suspended in 2ml of PRMT/$CaCl_2$ and split between 2 PRMB (Transformation Media Table) plates (1ml/plate) which contain mannitol to avoid osmotic shock. Cells were then placed in a growth chamber for 4 days after transformation, and then transferred onto a selective medium hygromycin (+hygro) plate. After a week these cells were transferred onto a $PpNH_4$ plate to allow for continued growth and placed back on selective medium after another week. Plants that survived the two rounds of selection were then individually isolated and grown to check for their fluorescence expression under confocal microscope.

After a stable transformation, lines also needed to be “cured” of the antibiotic resistance and in order to remove potential extra copies of the gene of interest. These lines were cured by performing a transient transformation using NLS-Cre. For the transient transformation, a similar protocol to the stable transformation was used.

Briefly, liquied $PnNH_4$+8% mannitol +10mM $CaCl_2$ was prepared instead of using solid PRMT to re-suspend the protoplasts. NLS-Cre is a plasmid that carries the gene for an enzyme known as Cre recombinase and zeocin resistance. Cre recombinase is able to bind to and cut out repeated *loxP* sites that flank the antibiotic resistance cassette and may have been inserted multiple times into the genome during the stable transformation. Once cured with Cre recombinase, the *P. patens* cells express only one copy of the gene of interest. This can be monitored by the loss of their hygromycin resistance phenotype.

The plants that survived the selection were then transferred into both a $PpNH_4$ plate and $PpNH_4$ plate containing hygromycin. Plants that have been successfully cured do not grow on hygromycin and were recovered from the $PpNH_4$ plate.

Table 4: Compositions of Transformation Media

Medium Name	**Composition**
MMg buffer	0.4M mannitol 15mM $MgCl_2$ 4mM MES (pH 5.7)
PEG4000/Ca2+	60% (w/v) PEG4000 0.8M mannitol 0.01M $CaCl_2$
W5 buffer	154mM NaCl 125mM $CaCl_2$ 5mM KCl 2mM MES (pH 5.7)
Plating medium – $PpNH_4$	1.03mM $MgSO_4$ 1.86mM KH_2PO_4 3.3mM $Ca(NO_3)_2$ 45mM $FeSO_4$ 9.93mM H_3BO_3 220nM CuSO4 1.966mM $MnCl_2$ 231nM $CoCl_2$ 191nM $ZnSO_4$ 169nM KI 103nM Na_2MoO_4 2.72mM diammonium tartrate
PRM-B	$PpNH_4$ with 6% (w/v) mannitol,0.8% (w/v) agar, 10 mM $CaCl_2$

3. Results

As previously mentioned, Rab 11 in animal and Ypt32 in yeast are both known to interact with myosin Vs, the homologs of the plant myosin XIs. Based on previous phylogenetic study (Agar, 2013), the closest moss homologs of Rab 11 and Ypt32 are the RabA family proteins. These Rabs have been narrowed down to RabA21, RabA4, and RabA53 which represent each one of the three RabA family subgroups that are present in *P. patens* and which all partially localize at the tip of caulonemal cells. To further study the role of myosin XI and these three Rabs in moss tip growth, two complementary strategies were designed. The first strategy consists of determining if myosin XI co-localizes with these Rab proteins at the same apical domain and of describing their temporal relationship by performing fluctuation cross correlation analysis. The second strategy is based on a biochemical approach to test for physical interaction between myosin XI and Rabs. This requires the generation of new constructs and is being presented in the second part of this manuscript.

3.1 Analysis of Spatial and Temporal Relationship between Myosin XI and RabA21 and between F-actin and RabA21

3.1.1 Myosin XI and RabA21 Intensities Fluctuate in Phase at the Tip of Caulonemal Cells

In order to determine if RabA21 co-localizes to the same apical domain as myosin XI in the tip growing caulonemal cells, two different lines were imaged under the confocal microscope. The first line (referred to as 3mEFGP-Myosin+3mCherry-

RabA21), expressed a 3mEGFP tag fused to the N-terminus of myosin and a RabA21 N terminus-tagged with a 3mCherry. The other line (referred to as Myosin-3mEGFPKI+3mCherry-RabA21), expressed a 3mEGFP tag directly inserted at the locus after the C terminus of the endogenous myosin gene. Only rapidly growing caulonemal cells which are known to accumulate F-actin, Myosin XI and the vesicle marker VAMP at their tip were imaged (Vidali et al 2010; Furt et al 2013).

As described in the material and methods section, kymographs were produced by averaging the fluorescent intensity at the apex of the cell over time. The linear slope of these kymographs were then used to determine the average growth rate of each cell analyzed. Both the 3mEFGP-myosin and myosin-3mEGFP-KI lines growth rates averaged in range with each other (Table 5), indicating that overexpressing a N-terminus fluorescently tagged myosin XI construct did not affect the growth rate of the caulonemal cells when compared with a line expressing a fluorescently tagged myosin XI at the endogenous level. These results are consistent with previously reported growth rates in transgenic lines (Table 5, Furt et al 2013) and non-transgenic lines (5.5 +/-0.6 nm/sec, Menand et al. 2007).

Table 5: Average growth rates of caulonemal cell lines calculated from kymographs measuring average fluorescent intensity at the apical tip over time

Lines	Number of Cells	Growth Rate (nm/sec)	Source
3mEGFP-myosin + 3mCherry-RabA21	6	6.87 ± 1.20	This paper
myosin-3mEGFP + 3mCherry-RabA21	6	5.15 ± 0.56	This paper
mEGFP-Lifeact + 3mCherry-RabA21	6	5.28 ± 0.99	This paper
3mEGFP-myosin + 3mCherryVamp	7	3.49 ± 0.42	(Furt et al., 2013)
3mEGFP-myosin + 3mCherry-Lifeact	12	3.78 ± 0.59	(Furt et al., 2013)

As shown in figures 6, 7 and 9, 3mCherry-RabA21 accumulates at the tip of caulonemal cells in both lines. This confirms the RabA21 localization that was previously observed in the single lines 3mEGFP-RabA21 and 3mCherry-RabA21 before the start of this project (Agar, 2012). Furthermore, the merged pictures show that both myosin and RabA21 co-localize to the same apical domain. Interestingly, the 3mCherry-RabA21 apical intensity fluctuates over time, which has been previously shown for myosin XI, F-actin and VAMP in other lines (Vidali et al 2010; Furt et al 2013).

To further characterize these fluctuations and compare them with those of myosin XI, the intensities of myosin XI and RabA21 were measured at the apical tip of the cell. The background intensities were then subtracted out, and the resulting ratio values of the intensity were normalized and plotted over time (Figure 6 and 7). These figures

show the overall fluctuations of one representative cell for each line over a 1000-2000s period of time as well as a 300-500s period in order to better observe the visual patterns of both signals. This analysis showed clear fluctuations of both myosin XI and RabA21 signals. The intensity peaks of both signals appeared to closely mimic each other.

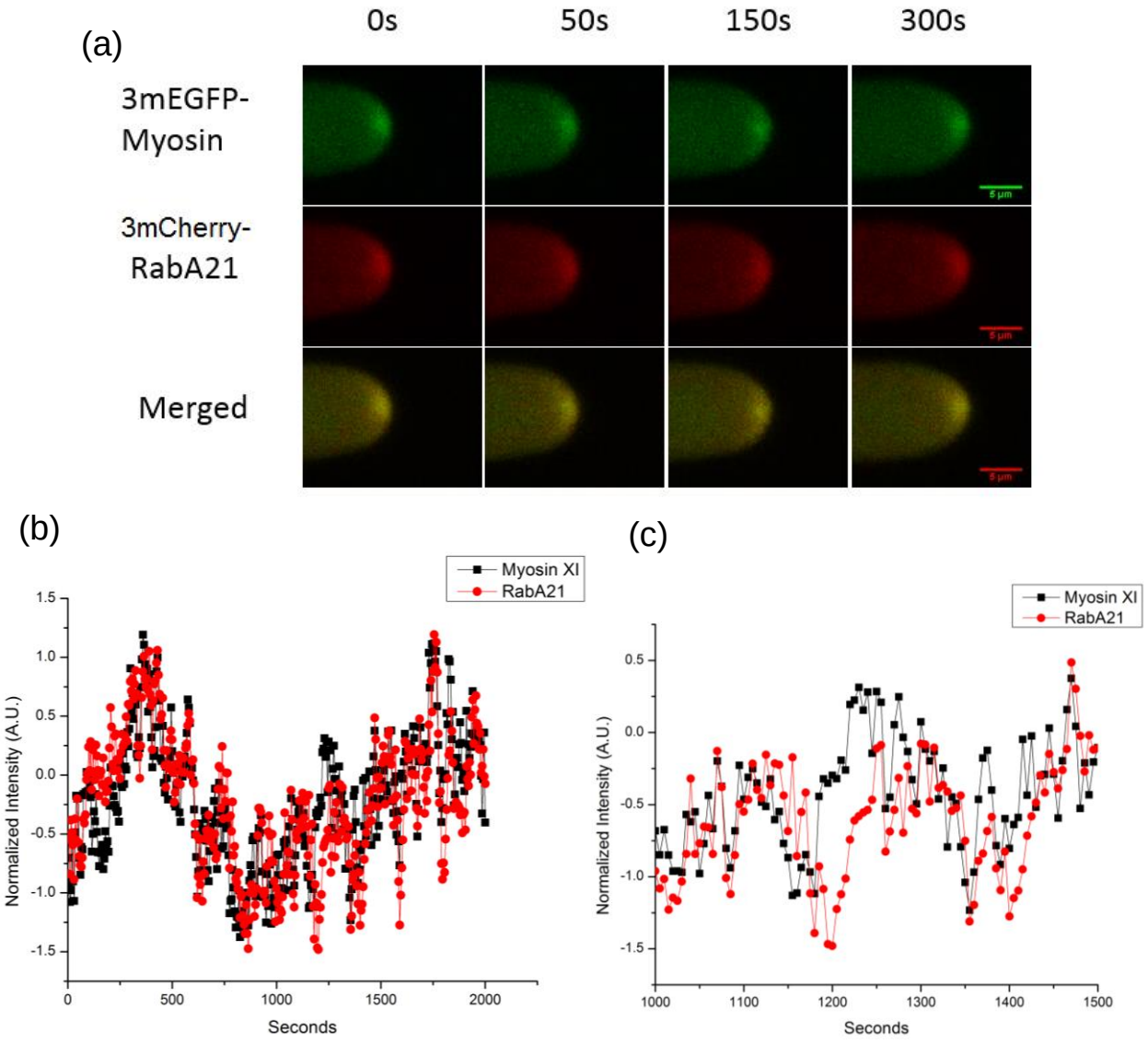

Figure 6: Dynamics of 3mEGFP-myosin XI and 3mCherry-RabA21 at the cell's apex.

(a) Distribution of 3mEGFP-myosin XI and 3mCherry-RabA21 by confocal microscopy. Average projections are shown in the top two panels and the merged image in the third one with myosin XI in green and RabA21 in red. The time (in seconds) at which each image was taken is shown at the top. (b) Intensity changes of 3mEGFP-myosin XI and 3mCherry-RabA21 at the apical region of the growing cell. (c) Enlarged region taken from panel b.

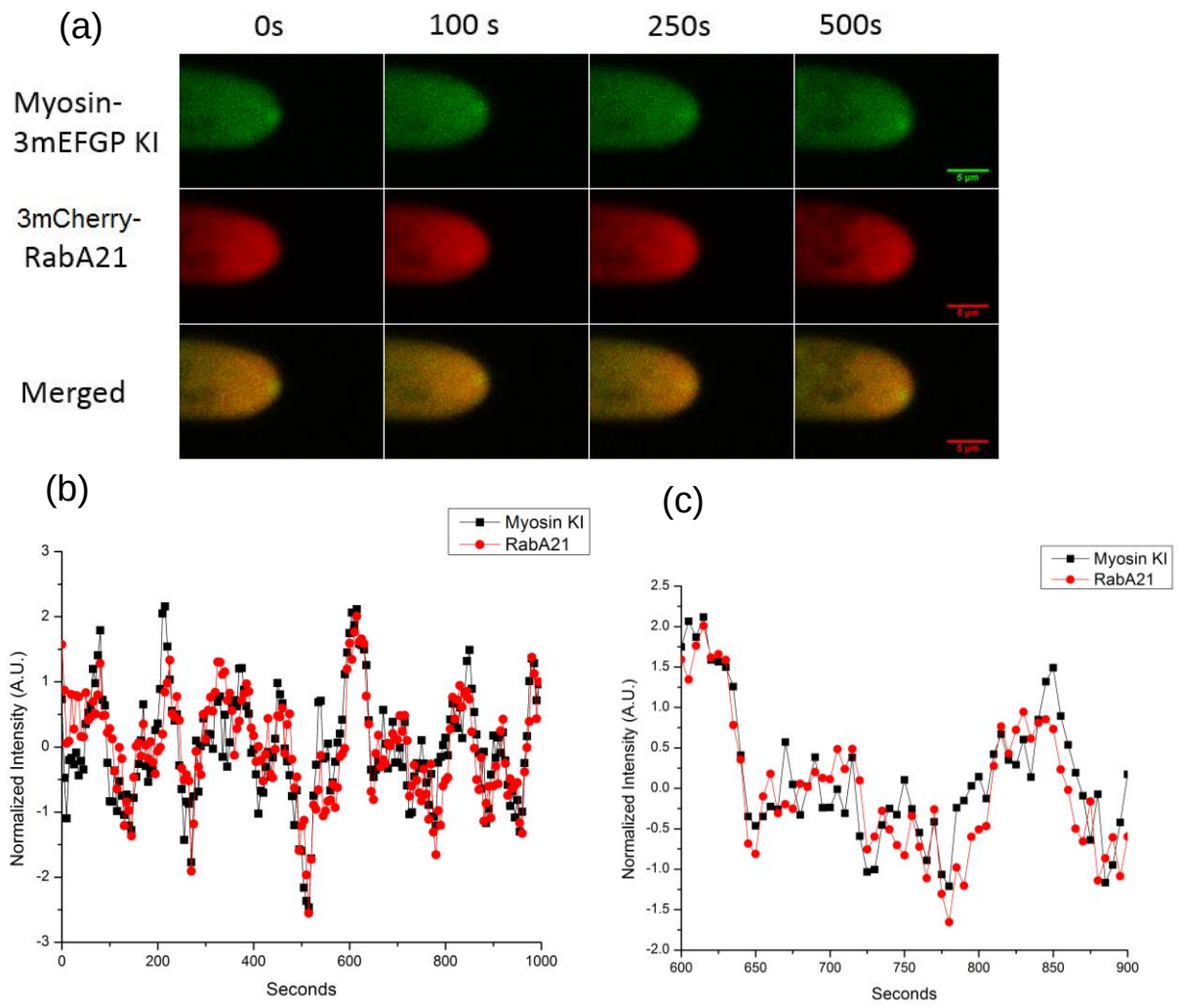

Figure 7: Dynamics of myosin XI-3mEGFP-KI and RabA21 at the cell's apex.

(a) Distribution of myosin XI-3mEGFP-KI and 3mCherry-RabA21 by confocal microscopy. Average projections are shown in the top two panels and the merged image in the third one with myosin XI in green and RabA21 in red. The time (in seconds) at which each image was taken in shown at the top. (b) Intensity changes of myosin XI-3mEGFP-KI and 3mCherry-RabA21 at the apical region of the growing cell. (c) Enlarged region taken from panel b.

To determine whether or not these fluctuations oscillated in or out of phase with one another, a cross correlation analysis was performed. Briefly, the phase relation of one signal was compared against the other at each time shift to produce a correlation coefficient, which could then be plotted over time (Figure 8). In all cells analyzed for both cell lines (n=6), the maximum correlation coefficient was obtained for a time shift

equal to zero between the two signals. This indicated that the fluorescent intensities of myosin XI and RabA21 fluctuate in phase with one another at the tip of growing caulonemal cells.

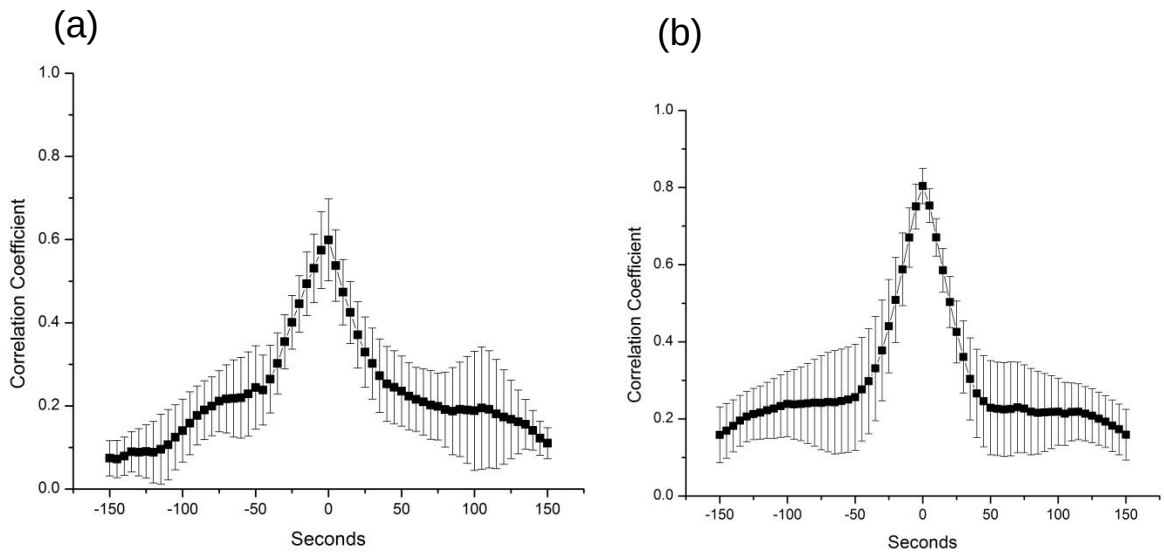

Figure 8: Phase analysis of myosin XI and RabA21; error bars correspond to the standard error of the mean; n=6 for both (a) analysis of myosin XI-3mEGFP-KI vs. RabA21 (b) analysis of 3mEGFP-myosin XI vs. RabA21

3.1.2 Apical RabA21 Anticipates F-actin at the Tip of Caulonemal Cells

It was previously shown that myosin XI signal precedes that of F-actin at the tip of caulonemal cells (Furt et al 2013). To determine whether or not RabA21 shows the same relationship toward F-actin, a third cell line was generated, in which RabA21 was tagged with 3mCherry and actin was labeled using a 3mEGFP tagged Lifeact, a high affinity actin binding protein. The calculated growth rate of the caulonemal cells of this cell line are in agreement with those reported for the two other transgenic lines and the non-transgenic lines (Table 5).

As expected and shown in figure 9, both 3mCherry-RabA21 and mEGFP-Lifeact accumulate at the tip of growing caulonemal cells and fluctuate over time. To gain further insight in the relationship between F-actin and RabA21, the intensities of actin and RabA21 were measured at the cell apex. Once again the resulting ratio values of the intensity were normalized and plotted over time (Figure 9). Similarly, this figure shows the overall fluctuations of one analyzed cell over a 2500s period of time as well as a 500s period of time in order to better observe the visual patterns of both signals. This analysis showed clear fluctuations of both actin and RabA21 signals. Once again, the intensity peaks of both signals appeared to closely mimic each other.

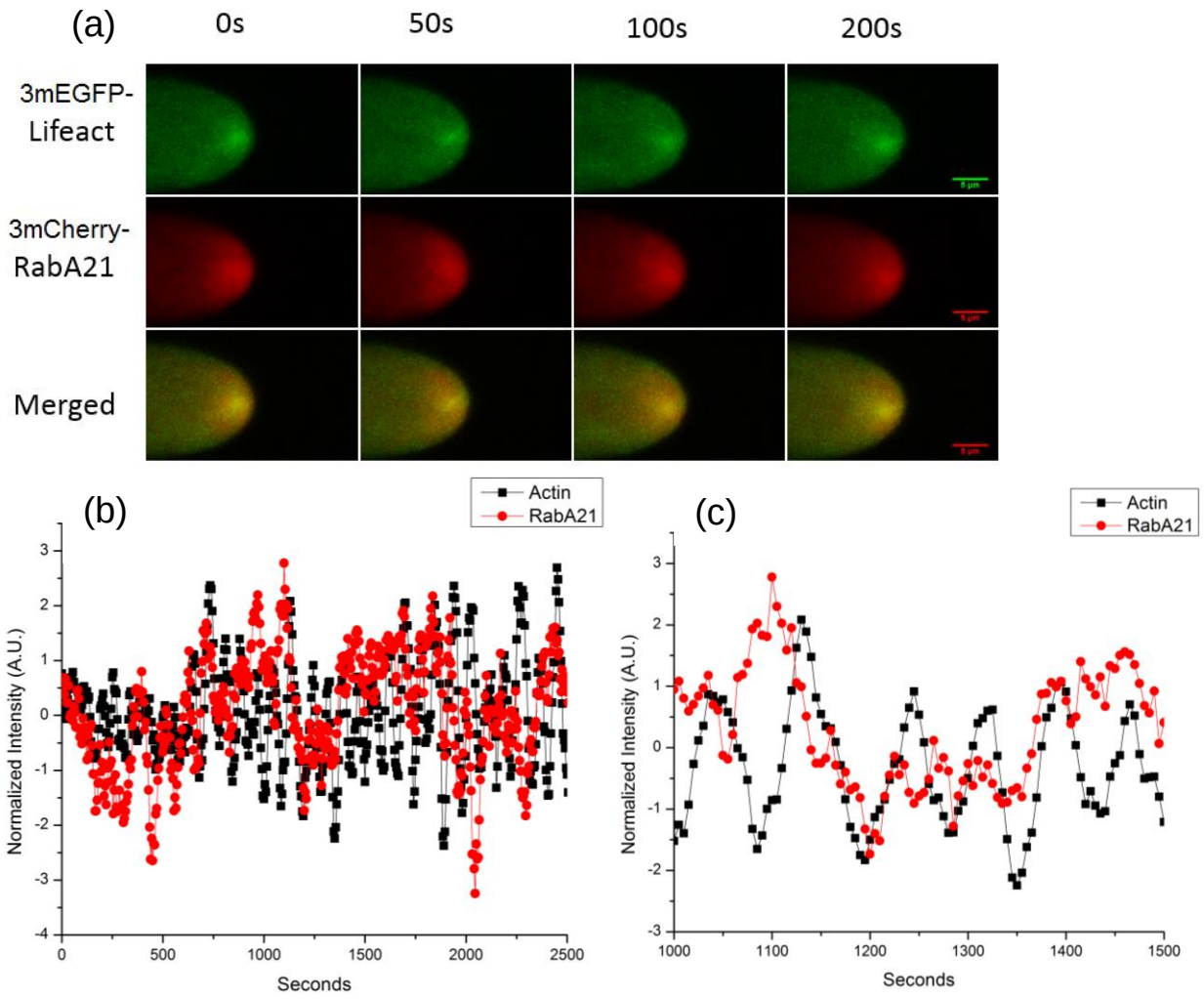

Figure 9: Dynamics of actin and RabA21 at the cell's apex.

(a) Distribution of 3mEGFP-Lifeact and 3mCherry-RabA21 by confocal microscopy. Average projections are shown in the top two panels and the merged image in the third one with Lifeact in green and RabA21 in red. The time (in seconds) at which each image was taken in shown at the top. (b) Intensity changes of Lifeact and 3mCherry-RabA21 at the apical region of the growing cell. (c) Enlarged region taken from panel b.

A time shift cross correlation analysis was again performed in order to determine whether or not these signals oscillated in or out of phase with one another (Figure 10). In this case, the signals of RabA21 and actin were out of phase with one another. For all cells analyzed (n=6), the average phase relation of RabA21 compared to actin was 20 ±

1.29 seconds. This means that the signal of RabA21 preceded and led the signal of actin, as it was previously demonstrated for myosin XI. Furthermore, the delay between the two signals is comparable in both lines (rab and actin: 20 ± 1.29 [Figure 10] vs myosin and actin: 16.25 ± 5.2 [Figure 12]).

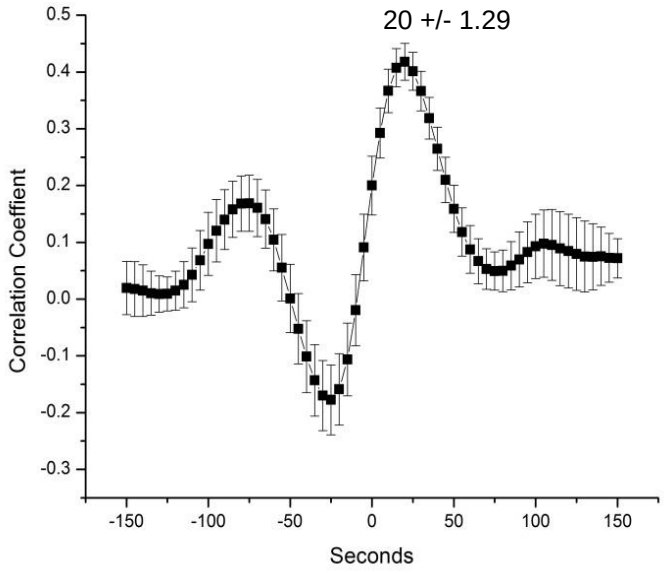

Figure 10: Phase analysis of actin and RabA21; error bars correspond to the standard error of the mean; n=6

3.2 Confirming De-trending Analysis Technique

In a previous study (Furt et al., 2013), fluctuation cross correlation analyses were performed to determine the spatial and temporal relationship of either actin and myosin or myosin and VAMP (a vesicle marker) at the growing apical tip of caulonemal cells. In this original analysis, a singular spectrum analysis was used for the de-trending algorithm of the oscillating data. This algorithm was taken from the KSpectra Toolkit and is based on advanced concepts from linear algebra and statistics, which are used to

trace the oscillation signals. The overall shape of these signals forms a slope or trend, which must be removed for proper analysis. These signals are de-trended by removing components from this recreation, allowing removal of the slope and creating a more horizontal function. For this study, a first mode Fourier de-trending algorithm was used. This algorithm utilizes the sum of sine and cosine equations in order to trace the original signal. The first of these equations or modes is a sinusoid that follows the overall sloping shape of the signal. Consecutive modes continue to follow the shape with increasing frequency. When the first mode is removed, the remaining sine and cosine equations create the horizontal function used to determine phase relation.

In order to confirm the validity of this new analysis (Fourier de-trending algorithm), data was taken from the previous study (Furt et al., 2013) and re-analyzed using the new de-trending method. The results from this previous study could be reproduced using this method, confirming its ability to produce reliable data as shown below.

3.2.1 Apical Myosin XI is in Phase with VAMP

Using this new program, the fluctuating intensities of myosin XI and VAMP were measured at the apical tip. Figure 11 shows the oscillating intensities along with the correlation analysis of these two signals. In all cells analyzed (n=7), the phase relation of these two signals was zero, indicating that the two proteins were completely in phase with one another without needing to shift either signal. This is comparable to the original

study in which the average phase relation was calculated at $6.7 \times 10^{-4} \pm 4.2 \times 10^{-4}$ sec (Furt et al., 2013).

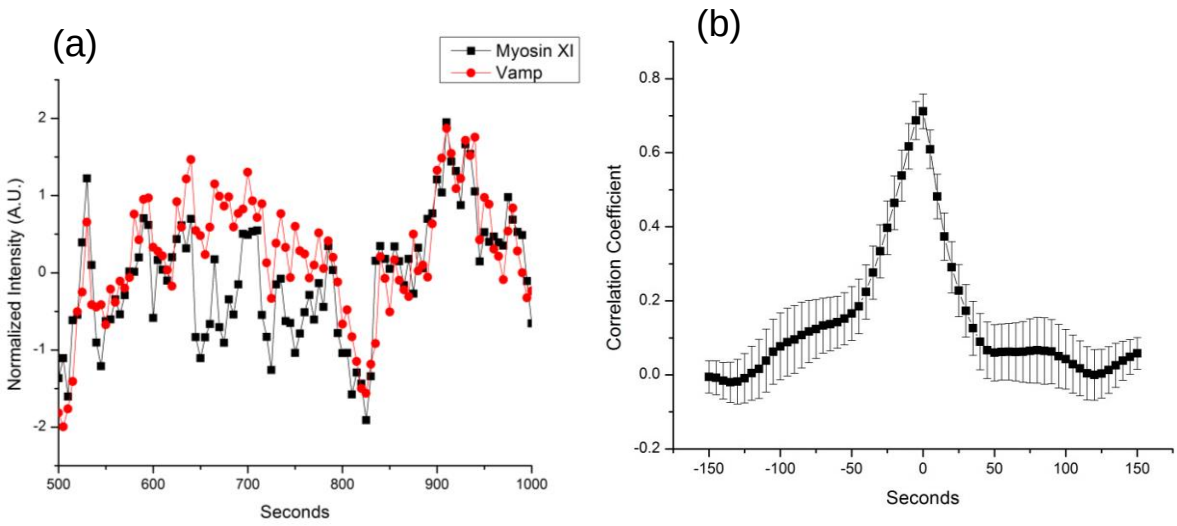

Figure 11: (a) Signal intensities of fluorescently tagged myosin XI and Vamp (b) Average cross correlation coefficient of Myosin + Vamp signals (n=7)

3.2.2 Apical Myosin XI Anticipates F-actin

Similarly, the fluctuating intensities of fluorescently tagged actin and myosin were analyzed and graphed over time. Figure 12 shows the oscillating intensities along with the correlation analysis of these two signals. In this case, the signals of actin and myosin correlated out of phase with one another. For all cells analyzed (n=12), the average phase relation of myosin compared to actin was 16.25 ± 5.2 seconds. This result compared similarly to the original study in which the average phase relation determined to be at 18.6 ± 1.7 sec (Furt et al., 2013).

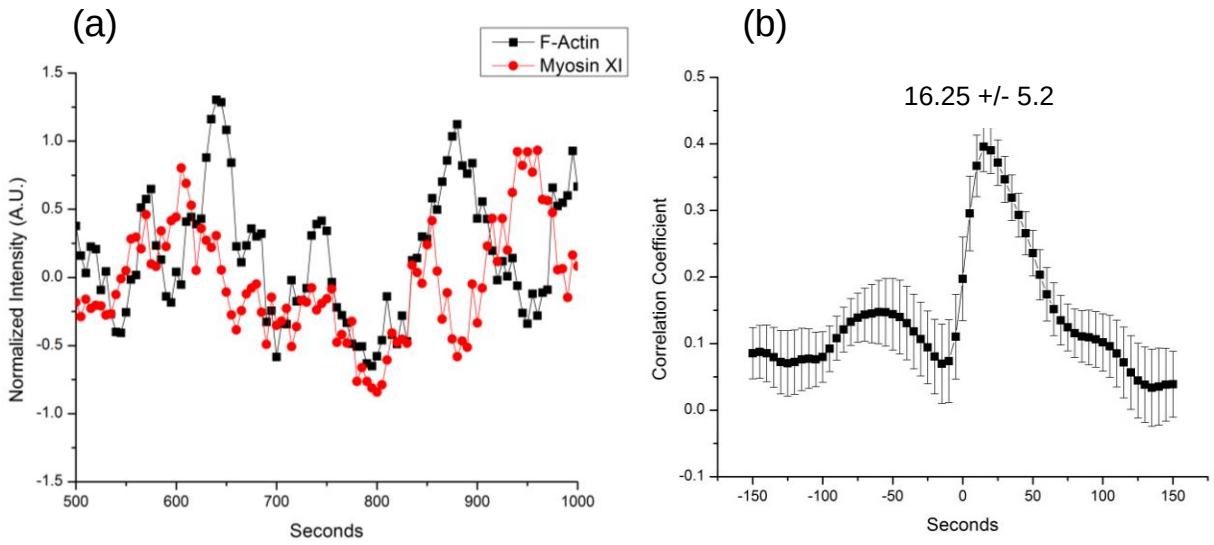

Figure 12: (a) Signal intensities of fluorescently tagged F-actin and myosin XI (b) Average cross correlation analysis of Actin + Myosin signals (n=12)

3.3 Generating Additional Stable Lines to Characterize the Role of Myosin XI and Rab Proteins in Moss Tip Growth

Along with analyzing the correlation between RabA21 and myosin/actin, there are additional RabA proteins that are known to localize at the tip caulonemal cells in *P. patens*. One of these is a Rab known as RabA53. In order to analyze RabA53 and compare it with myosin and actin, transgenic lines must first be produced in which both RabA53 and either myosin or actin are fluorescently tagged.

To start, a line containing Myosin-3mEGFP-KI was transformed with 3mCherry-RabA53 DNA. This transformation produced one successful clone that expressed both fluorescent markers under the microscope (Figure 13). However because only one potential clone was formed, additional transformations are required.

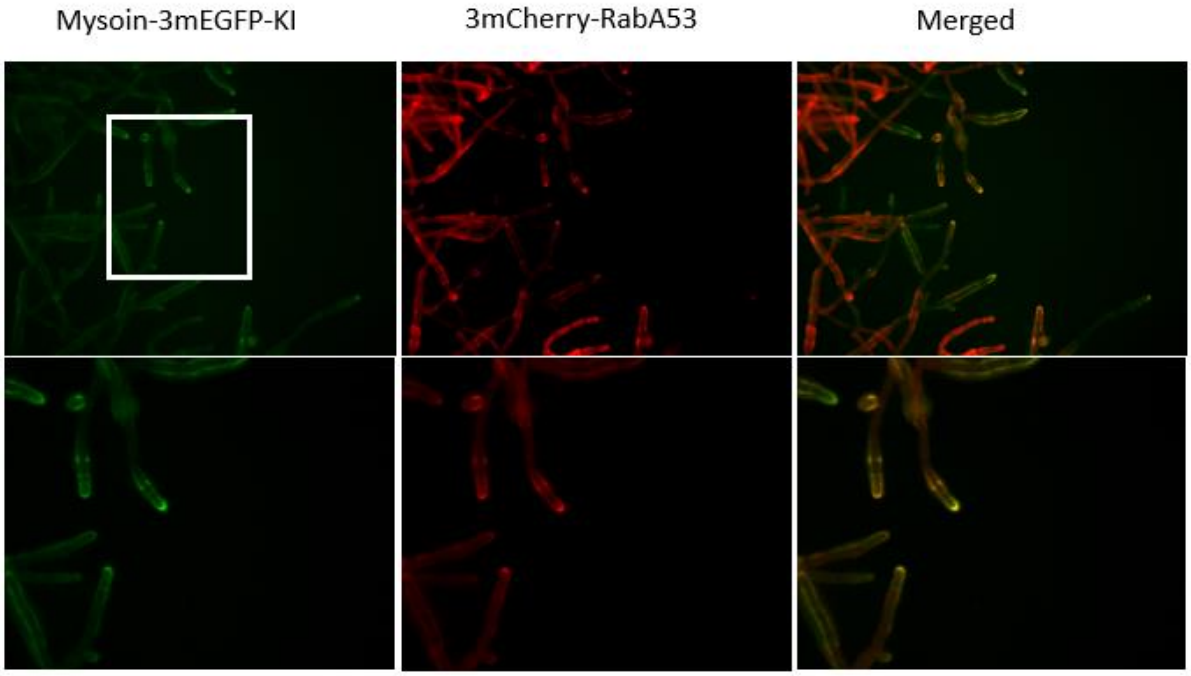

Figure 13: Fluorescent images of Myosin-3mEGFP-KI+3mCherryRabA53 line at 10x; Green channel (left) shows 3mEGFP expression, Red channel (center) shows 3mCherry expression, these two channels were then merged (right) in order to show both fluorescent markers were being expressed in the same cell; white box indicates zoomed area (bottom)

3.4 Generating GST-tagged RabA21, RabA4, and RabA53 Constructs for Protein-Protein Interaction Study

In order to determine if the myosin protein is directly binding to a Rab protein, a pull down assay can be performed. In this assay, proteins of interest are fused to a specific tag protein, which contains a high affinity for binding to beads present in a purification column. Once the Rab is bound to the column, purified myosin globular tail constructs will be passed through the column in order to determine whether or not these two proteins bind.

To perform these experiments, new constructs needed to be generated in which the three different types of RabA (RabA21, RabA4, and RabA53) present in *P. patens* are recombined with a GST (Glutathione S-transferase) tag protein capable of high affinity binding with glutathione beads. In order to accomplish this, mRNA was first isolated and purified from a *P. patens* Gransden line to generate cDNA. It was necessary to use cDNA instead of moss genomic DNA because bacteria do not contain the proper functions required to remove introns and splice together exons to make the appropriate transcripts. Using reverse transcriptase (RT), moss mRNA was converted to cDNA in order to avoid the presence of introns. Different concentrations of this cDNA template were then used in a PCR reaction, with appropriate primers to amplify RabA21 (see material and methods), in order to determine the concentration that would result in the optimal DNA yield. These PCR products obtained using varying cDNA concentrations were then ran through an agarose gel (Figure 14). From this gel, cDNA at 2ug and 250ng yielded thicker bands of DNA at the appropriate size of 709 bp (cDNA + Att sites). The positive control in lane 2 did not appear because the measured concentrations that were used were incorrect.

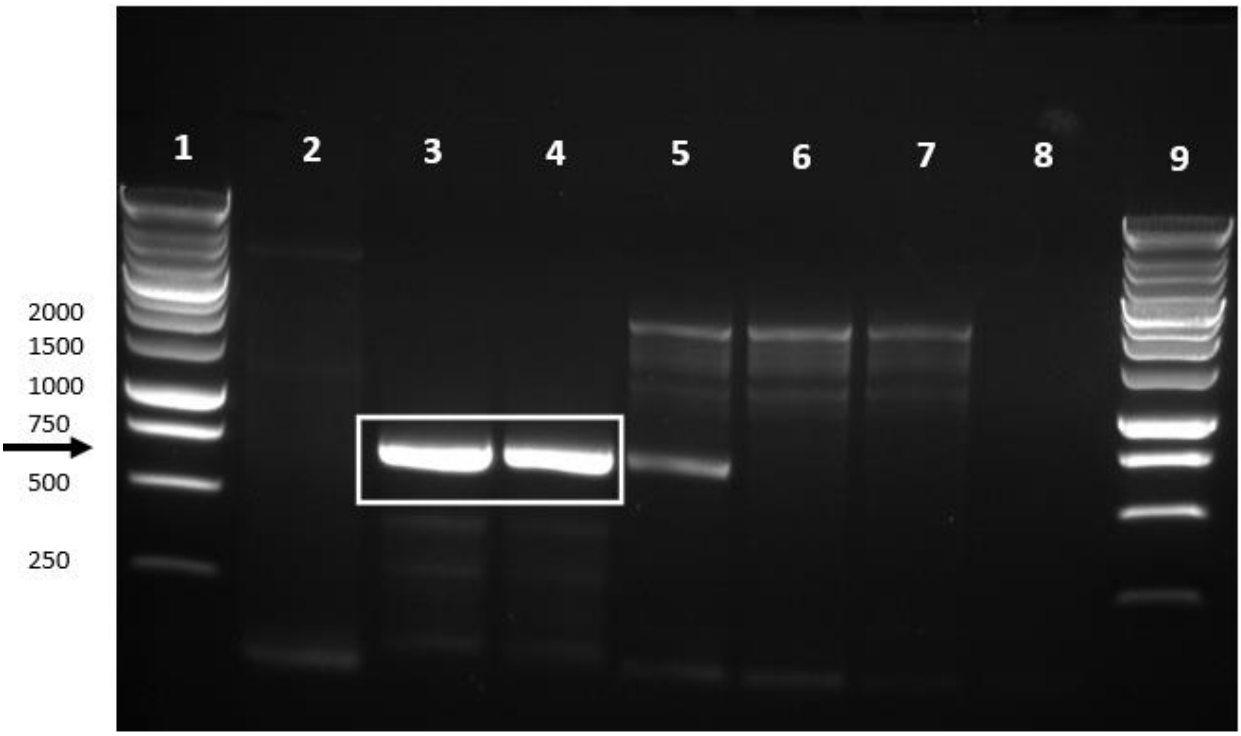

Figure 14: PCR products obtained using cDNA template and RabA21 primers. Lanes 1+9=Ladder, 2=Positive Control, 3= 2ug cDNA, 4=250ng cDNA, 5= 2.5ng cDNA, 6=250pg cDNA, 7= 25 pg cDNA, 8=H_2O, negative control; arrow indicates the expected band size for RabA21 + Att sites; boxed area indicates correct bands

For the next experiment, I choose to use 259ng of cDNA as template to amplify the cDNA of RabA21, RabA4, and RabA53 using the appropriate primers (see material and methods). These three separate PCR products were then run through an agarose gel along with a control containing only water and the corresponding primers (Figure 15). Bands for RabA21, RabA4, and RabA53 were located at 709, 727, and 710 bps respectively, and each band was cut out and the DNA was extracted from the gel.

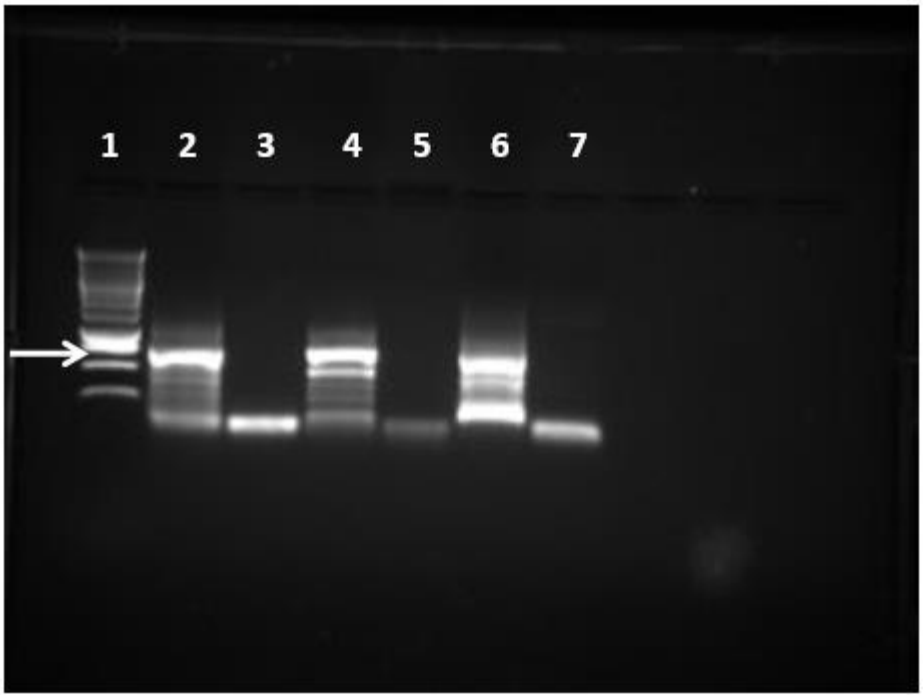

Figure 15: PCR using cDNA template and RabA21, RabA4, and RabA53 primers, Lanes 2, 4, and 6 contain cDNA + RabA21, RabA4, and RabA53 primers respectively; Lanes 3, 5, 7 are controls that contain H_2O + primers

Using the Gateway system, these PCR products were then inserted into different entry and destination vectors via homologous recombination (Methods: Figure 5). First a BP reaction was performed in order to recombine the fragment into the pDONR P1P2 entry clone plasmid. These BP reaction products were then transformed into *E. coli*, isolated using a mini-prep, and then screened and sequenced. The plasmids were screened by using restriction enzymes that cut the DNA at specific locations. The size of the resulting DNA fragments were then determined by running the reaction through a gel. Figure 15 shows an example of one these gel screenings in which different clones of RabA21 and RabA4 that were cut near their ATT sites located at the either end of the inserted gene. Restriction digestions for RabA53 were also performed (data not shown). Bands in all three RabA plasmids were expected at approximately 2300bp and 800bp

(Table 6, Figure 16a). Digested plasmids that contained the appropriately sized bands confirm that an insert of the correct size is located in the plasmid. However, there is a very small chance that a different, similarly sized insert other than Rab, was placed inside the plasmid. Therefore a second screening was also performed for all three RabAs in which a site located in the middle of the Rab insert was cut. For this second screening, bands in all three RabA plasmids were expected at approximately 2600bp and 600bp (Table 6, Figure 16b). Plasmids that passed both these screenings were then sequenced in order to confirm that they contained in proper inserted RabA gene and that no mutations on the gene were present. The program Vector NTI was used to analyze and confirm the appropriate sequences these plasmids.

Table 6: Restriction Enzymes used to screen entry clones

pDONR 221 inserts	Restriction Enzymes	Expected Band Size (bp)
RabA21	EcoRV + AflII EcoRV + KpnI	2317 + 878 2655 + 540
RabA4	EcoRV + AflII EcoRV + EcoRI	2317 + 896 2584 + 629
RabA53	AflII + EcoRV NcoI + EcoRV	2317 + 878 2591 + 604

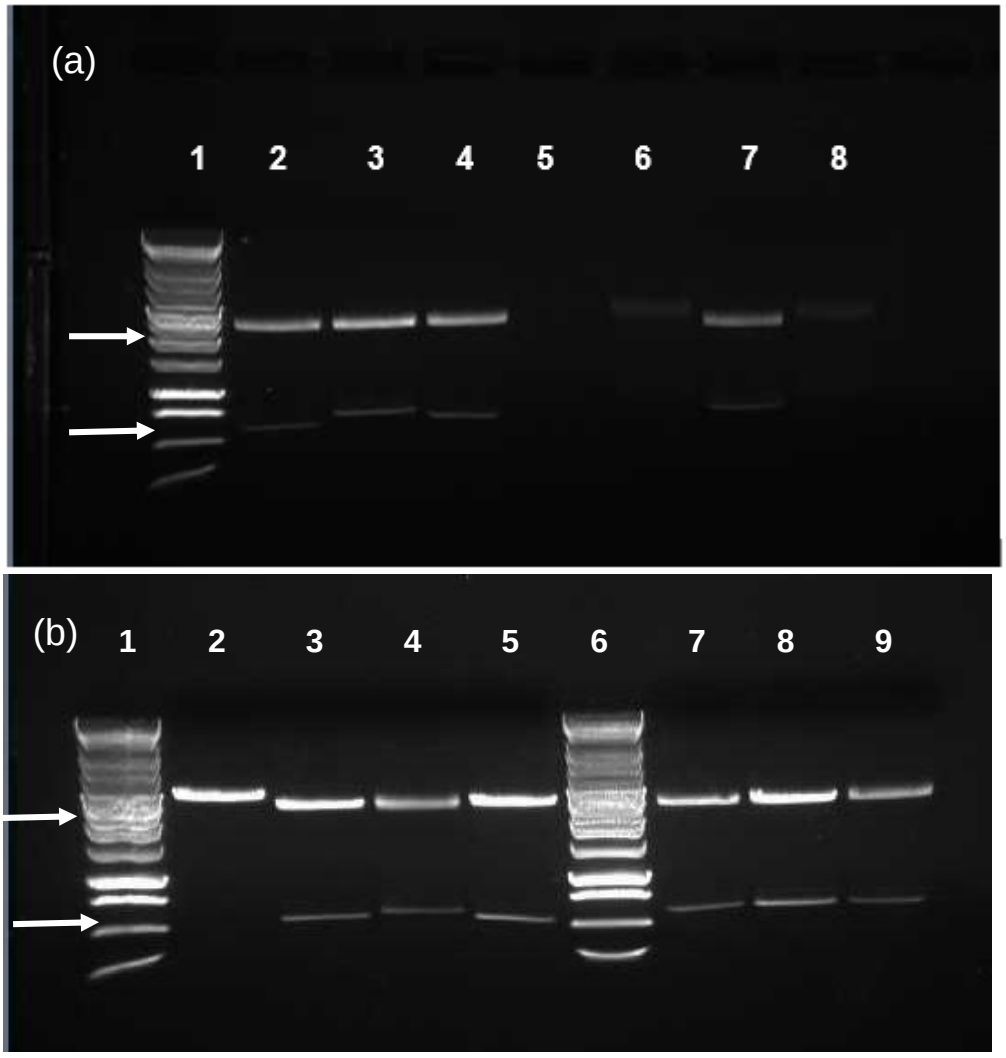

Figure 16: (a) First screening in which entry plasmids were cut just outside gene insert, Lanes 2-4: RabA21, Lanes 6-8: RabA4 clones; (b) Second screening in which entry plasmids were cut inside gene insert Lanes 2-5: RabA21, Lanes 7-9: RabA4; arrows indicate approximate locations of expected bands

Once proper entry clones were made and confirmed, LR reactions were then performed in order to place the inserted gene into a destination vector containing the GST tag. These plasmids were again transformed using *E.* coli, isolated using a mini-prep, and then screened and sequenced. For screening, only one series of restriction

digestions were performed (Table 7). This is because there was no appropriate restriction enzyme that could cut a site inside the Rab gene without cutting multiple sites on the plasmid. Figure 16 shows one of the resulting gels from this screening. Both bands appeared for some of the RabA21, RabA4 and RabA53 plasmids. Because these bands were faint, contrast of the image was enhanced in order to visualize them. Plasmids that passed this screening were selected and then sequenced in order to confirm the presence of any of the three RabA inserts along with GST tag. Again, the program Vector NTI was used to analyze and confirm the appropriate sequences these plasmids. These plasmids are now capable of being transformed and expressed in a strain of *E. coli* optimized for overexpression of recombinant proteins.

Table 7: Restriction Enzymes used to screen destination vector clones

pDEST-GST	Restriction Enzymes	Expected Band Size (bp)
RabA21	BamHI + Ncol	5280 + 729
RabA4	BamHI + Ndel	4606 + 1421
RabA53	BamHI + Ndel	4606 + 1403

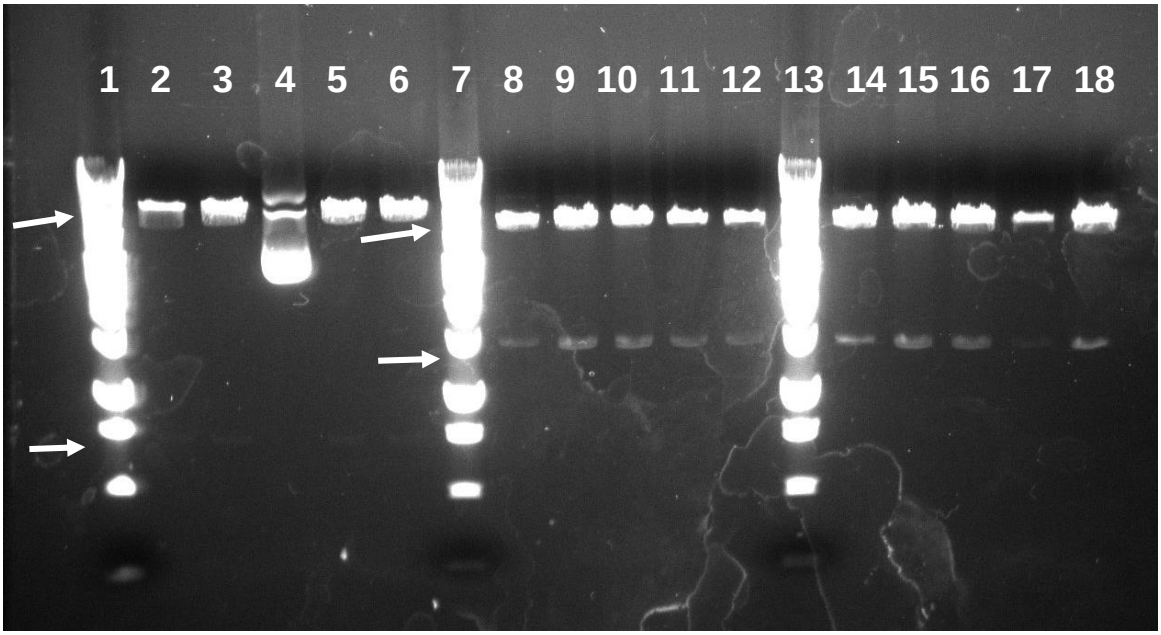

Figure 16: Destination plasmids cut just outside gene insert, Lanes 2-6: RabA21; Lanes 8-12: RabA4 clones; Lanes 14-18 RabA53; arrows indicate approximate locations of expected bands

4. Discussion and Suggestions for Future Study

The purpose of this study was to determine the molecular mechanism behind polarized tip growth in plants. It has previously been determined that the motor protein myosin XI is essential for polarized tip growth (Vidali et al., 2010). It is commonly accepted that part of myosin XI function is to assist in this process by transporting secretory vesicles containing cell wall materials along actin filaments to the tips of growing cells. To be able to identify and transport these vesicles, myosin must be able to interact with proteins located on the surface of these vesicles. This interaction has been demonstrated in animal and yeast cells where class V myosins homologous to myosin XI have been shown to interact with RabA family proteins on post-Golgi vesicles and membrane compartments (Wu et al., 2002; Lipatova et al., 2008). This interaction has not yet been shown in plants. Therefore it was hypothesized that myosin may interact with a small GTPase protein belonging to the Rab family. The results from this study seek to test myosin XI in *P. patens* interacts, either directly or indirectly, with one of the RabA proteins during polarized tip growth.

As part of this work, a previous study that examined the interaction between myosin, VAMP, and actin the tip of growing cells was re-analyzed (Furt et al., 2013). This was done so that the results from the previous study could be directly compared with the results obtained from examining the relationship between myosin XI, RabA21, and actin. Using a vesicle marker known as VAMP (a v-SNARE), this prior study demonstrated that myosin XI was associated with secretory vesicles at the growing tip.

Both protein signals were highest at the tip of these cells and their intensities fluctuated in phase with one another over time. In addition, F-actin was also found to be concentrated at the tip of growing cells and fluctuate over time. However, myosin XI and F-actin signals fluctuated slightly out of phase with one another, with the myosin signal preceding and anticipating the signal of actin. This was an interesting result in that it suggests that myosin may be involved in actively recruiting and organizing these growing actin filaments. In this study, new analysis of these previous data confirmed and reproduced these results.

Similar to myosin and actin, RabA21 was shown to localize at the tip of caulonemal cells. The signal intensity of RabA21 also fluctuated at the growing tip of these cells over time. Along with being localized at the tip of the cell, if two proteins such as myosin and RabA21 interact with one another, it would be expected that these fluctuating signals would also correlate and be in phase. RabA21 was found to correlate with myosin completely in phase. And similar to myosin, RabA21 preceded F-actin by approximately 20 seconds; myosin was shown to precede F-actin by a similar time range (16.25 +/- 5.2 seconds). This correlation provides strong evidence that RabA21 is at the same compartment with myosin XI at the tip of growing caulonema cells.

In this study, only RabA21 was analyzed at the tip and its temporal and spatial dynamics compared with myosin and actin. However, a different *P. patens* RabA that belongs to the RabA5 subfamily (RabA53), was also found to be localized at the tip of growing caulonemal cells. Because of its location at the tip, RabA53 may be another candidate for myosin interaction during polarized growth in *P. patens*, but additional

cross correlation analyses will be required to determine if this is the case. To evaluate this, double lines could be constructed that contained both fluorescently tagged myosin XI and RabA53. Once these lines are produced, the fluorescent signals could be similarly analyzed in order to observe the correlation between these two proteins.

Cross correlation analysis only determines whether or not proteins signals correlate with one another. This is important because correlation of protein signals provides evidence that these two proteins may be interacting with one another, or be at the same compartment at the same time. This interaction can further be proven by performing co-immunoprecipitation assays. However, neither method can prove whether or not this interaction is direct or indirect. In order to determine direct protein interactions, pull-down assays can be performed. Pull-down assays are a method that evaluates if two proteins interact and is based on principles of affinity chromatography, in which a bait protein in tagged and captured using a ligand with a high affinity for the tag. In this way, the bait protein along with any other proteins that interact with this protein can be isolated and analyzed.

For this study, three separate constructs were formed in which the three RabA proteins found in *P.* patens, RabA21, RabA4, and RabA53, were fused with a GST (Glutathione *S*-transferase) tag in order to perform this pull down assay. GST has a high affinity to bind to its substrate glutathione (GSH) and thus will bind to purification beads containing this substrate. In order to prepare these constructs, these three RabA proteins were isolated and fused to GST using the Gateway system. Consecutive screening and sequencing confirmed successful plasmids containing both the GST tag

and the appropriate RabA gene. The next step would then be to use these plasmids and transform them into *E. coli* for expression.

4.1 Conclusions

The high correlation between RabA21 and myosin XI fluctuations supports the hypothesis that the two proteins interact during polarized growth. This finding is strengthened by the additional evidence that the appearance of RabA21 precedes and anticipates the appearance actin in the same way myosin has been shown to precede and anticipate actin. However further testing is needed to determine direct interaction between myosin and Rab. Therefore genetic constructs were created in which the three different RabA proteins present in *P. patens* were recombined with a GST tag on the N terminus. Once expressed in bacteria and purified, these fusion proteins can be used for pull down assays that would prove or disprove a direct protein interaction with the myosin XI tail region. In doing so, the molecular mechanism and regulation of myosin binding to vesicles during polarized tip growth in plants can be better understood.

References:

Agar, E. (2013). Interactions between Myosin Xia and Rab Proteins in the Moss *Physcomitrella patens.* Worcester Polytechnic Institute; pp. 19.

Armstrong, E. (2012). Characterization of the Interaction Between Myosin XIa and RabA4 in *Physcomitrella patens*. Worcester Polytechnic Institute

Beike, A. and Rensing, S. (2010) The *Physcomitrella patens* genome-a first stepping stone towards understanding bryophyte and land plant evolution. *Tropical Bryology;* 31: 43-50

Furt, F., Liu, Y., Bibeau, J. P., Tüzel, E., & Vidali, L. (2013). Apical myosin XI anticipates F-actin during polarized growth of *Physcomitrella patens* cells. *The Plant Journal, 73*(3), 417-428. doi:10.1111/tpj.12039

Goffinet, B. and Shaw, A. (2009). Bryophyte biology. *Cambridge University Press.* 2nd Ed. ISBN: 9780521693226 (pbk.)

Hales, C. Vaerman, J. Goldenring, J. (2002). Rab11 Family Interacting Protein 2 Associates with Myosin Vb and Regulates Plasma Membrane Recycling. *The Journal of Biological Chemistry.* 277: 50415-50421, doi: 10.1074/jbc.M209270200

Hashimoto, K. Igarashi, H. Mano, S. Nishimura, M. Shimmen, T. Yokota, E. (2005). Peroxisomal Localization of a Myosin XI Isoform in *Arabidopsis thaliana. Plant & Cell Physiology.* 46 (5): 782-789 doi:10.1093/pcp/pci085

Holubcová, Z., Howard, G., & Schuh, M. (2013). Vesicles modulate an actin network for asymmetric spindle positioning. *Nature Cell Biology, 15*(8), 937-U380. doi:10.1038/ncb2802

Huber, F. Schnauß, J. Rönicke, S. Rauch, P. Müller, K. Fütterer, C. Käs, J. (2013) Emergent complexity of the cytoskeleton: from single filaments to tissue, *Advances in Physics*, 62:1, 1-112, DOI: 10.1080/00018732.2013.771509

Itoh, T., Watabe, A., Toh-E, A., & Matsui, Y. (2002). Complex formation with Ypt11p, a rab-type small GTPase, is essential to facilitate the function of Myo2p, a class V myosin, in mitochondrial distribution in *Saccharomyces cerevisiae*. *Molecular and Cellular Biology, 22*(22), 7744-7757. doi:10.1128/MCB.22.22.7744-7757.2002

Lipatova, Z. Tokarev, A. Jin, Y. Mulholland, J. Weisman, L. Segev, N. (2008). Direct Interaction between a Myosin V Motor and the Rab GTPases Ypt31/32 Is Required for Polarized Secretion. *Molecular Biology of the Cell.* 19(10): 4177-4187, doi: 10.1091/mbc.E08-02-0220

Liu, Y., & Vidali, L. (2011). Efficient polyethylene glycol (PEG) mediated transformation of the moss *Physcomitrella patens*. *Journal of Visualized Experiments: JoVE,* (50) 2560 doi: 10.3791/2560

Maravillas-Montero, J. L., & Santos-Argumedo, L. (2012). The myosin family: Unconventional roles of actin-dependent molecular motors in immune cells. *Journal of Leukocyte Biology, 91*(1), 35-46. doi:10.1189/jlb.0711335

Menand B, Calder G, Dolan L (2007). Both chloronemal and caulonemal cells expand by tip growth in the moss *Physcomitrella patens*. *Journal of Experimental Biology*. 58:1843–1849

Park, E., & Nebenführ, A. (2013). Myosin XIK of *Arabidopsis thaliana* accumulates at the root hair tip and is required for fast root hair growth. *PloS One, 8*(10), e76745. doi:10.1371/journal.pone.0076745

Peremyslov, V. V., Prokhnevsky, A. I., & Dolja, V. V. (2010). Class XI myosins are required for development, cell expansion, and F-actin organization in *Arabidopsis*. *The Plant Cell, 22*(6), 1883-1897. doi:10.1105/tpc.110.076315

Peremyslov, V. V., Morgun, E. A., Kurth, E. G., Makarova, K. S., Koonin, E. V., & Dolja, V. V. (2013). Identification of myosin XI receptors in *Arabidopsis* defines a distinct class of transport vesicles. *The Plant Cell, 25*(8), 3022-3038. doi:10.1105/tpc.113.113704

Rensing, S.A., Lang, D., Zimmer, A.D., Terry, A., Salamov, A., Shapiro, H., Nishiyama, T., Perroud, P.F., Lindquist, E.A., Kamisugi, Y., et al. (2008). The *Physcomitrella* genome reveals evolutionary insights into the conquest of land by plants. Science. 319, 64-69.

Schaefer, D. G., & Zrÿd, J. P. (1997). Efficient gene targeting in the moss *Physcomitrella patens*. *The Plant Journal: For Cell and Molecular Biology, 11*(6), 1195-1206.

Schuh, M. (2011). An actin-dependent mechanism for long-range vesicle transport. *Nature Cell Biology, 13*(12), 1431-U115. doi:10.1038/ncb2353

Seabra, M. C., & Coudrier, E. (2004). Rab GTPases and myosin motors in organelle motility. *Traffic, 5*(6), 393-399. doi:10.1111/j.1398-9219.2004.00190.x

Tóth, J. Kovács, M. Wang, F. Nyitray, L. Sellers, J. (2005). Myosin V from *drosophila* reveals diversity of motor mechanisms within the myosin V family. *Journal of Biological Chemistry, 280*(34), 30594-30603. doi:10.1074/jbc.M505209200

Vidali, L., & Bezanilla, M. (2012). *Physcomitrella patens*: A model for tip cell growth and differentiation. *Current Opinion in Plant Biology*, 15(6), 625-631. doi:10.1016/j.pbi.2012.09.008

Vidali, L., Burkart, G. M., Augustine, R. C., Kerdavid, E., Tüzel, E., & Bezanilla, M. (2010). Myosin XI is essential for tip growth in *Physcomitrella patens*. *The Plant Cell, 22*(6), 1868-1882. doi:10.1105/tpc.109.073288

Woollard, A. A. D., & Moore, I. (2008). The functions of Rab GTPases in plant membrane traffic. *Current Opinion in Plant Biology, 11*(6), 610-619. doi:10.1016/j.pbi.2008.09.010

Wu, X. Rao, K. Zhang, H. Wang, F. Sellers, J. Matesic, L. Copeland, N. Jenkins, N. Hammer, J. (2002) Identification of an organelle receptor for myosin-va. *Nature Cell Biology, 4*(4), 271-278. doi:10.1038/ncb670

Zhang, Y., & McCormick, S. (2010). The regulation of vesicle trafficking by small GTPases and phospholipids during pollen tube growth. *Sexual Plant Reproduction, 23*(2), 87-93. doi:10.1007/s00497-009-0118-z

Zerial, M., and McBride, H. (2001). Rab proteins as membrane organizers. (2001). *Nature Reviews Molecular Cell Biology, 2*(2), 107-117. doi:10.1038/35052055